Research Paper
J. Astron. Space Sci. 28(2), 123-132 (2011)
DOI: 10.5140/JASS.2011.28.2.123

JASS Journal of Astronomy and Space Sciences

Variation of Magnetic Field (B_y, B_z) Polarity and Statistical Analysis of Solar Wind Parameters during the Magnetic Storm Period

Ga-Hee Moon†

Daegu Science High School, Daegu 706-852, Korea

It is generally believed that the occurrence of a magnetic storm depends upon the solar wind conditions, particularly the southward interplanetary magnetic field (IMF) component. To understand the relationship between solar wind parameters and magnetic storms, variations in magnetic field polarity and solar wind parameters during magnetic storms are examined. A total of 156 storms during the period of 1997~2003 are used. According to the interplanetary driver, magnetic storms are divided into three types, which are coronal mass ejection (CME)-driven storms, co-rotating interaction region (CIR)-driven storms, and complicated type storms. Complicated types were not included in this study. For this purpose, the manner in which the direction change of IMF B_y and B_z components (in geocentric solar magnetospheric coordinate system coordinate) during the main phase is related with the development of the storm is examined. The time-integrated solar wind parameters are compared with the time-integrated disturbance storm time (*Dst*) index during the main phase of each magnetic storm. The time lag with the storm size is also investigated. Some results are worth noting: CME-driven storms, under steady conditions of $B_z < 0$, represent more than half of the storms in number. That is, it is found that the average number of storms for negative sign of IMF B_z (T1~T4) is high, at 56.4%, 53.0%, and 63.7% in each storm category, respectively. However, for the CIR-driven storms, the percentage of moderate storms is only 29.2%, while the number of intense storms is more than half (60.0%) under the $B_z < 0$ condition. It is found that the correlation is highest between the time-integrated IMF B_z and the time-integrated *Dst* index for the CME-driven storms. On the other hand, for the CIR-driven storms, a high correlation is found, with the correlation coefficient being 0.93, between time-integrated *Dst* index and time-integrated solar wind speed, while a low correlation, 0.51, is found between time-integrated B_z and time-integrated *Dst* index. The relationship between storm size and time lag in terms of hours from B_z minimum to *Dst* minimum values is investigated. For the CME-driven storms, time lag of 26% of moderate storms is one hour, whereas time lag of 33% of moderate storms is two hours for the CIR-driven storms. The average values of solar wind parameters for the CME and CIR-driven storms are also examined. The average values of $|Dst_{min}|$ and $|B_{zmin}|$ for the CME-driven storms are higher than those of CIR-driven storms, while the average value of temperature is lower.

Keywords: disturbance storm time index, magnetic storms, solar wind parameters

1. INTRODUCTION

It is generally believed that the occurrence of a magnetic storm depends upon the solar conditions, particularly the southward interplanetary magnetic field (IMF) component. Some researchers have suggested a relationship between magnetic storms and solar wind parameters (Weigel 2010). Wu & Lepping (2006) investigated geomagnetic activity induced by interplanetary magnetic cloud (MC) during the past four solar cycles, 1965~1998, and found that the intensity of geomagnetic storms is more severe in a solar active period than in a solar quiet period.

As suggested by some researchers, it is important to discuss the interplanetary drivers causing geomagnetic

Received Apr 02, 2011 **Revised** May 13, 2011 **Accepted** June 03, 2011

†**Corresponding Author**
E-mail: kafemoon@hanmail.net
Tel: +82-53-765-0012 Fax: +82-53-765-0023

storms. Echer et al. (2008) also identified the interplanetary causes of intense geomagnetic storms and their solar dependence occurring during the solar cycle 23 (1996~2006). They concluded that the most important interplanetary structures leading to intense southward B_z are MC, which drove fast shocks causing 24% of the magnetic storms, and sheath fields, which also caused 24% of the storms. Borovsky & Denton (2006) showed twenty-one differences between coronal mass ejection (CME)-driven storms and co-rotating interaction region (CIR)-driven storms by table. According to their findings, CME-driven storms have denser plasma sheets, stronger ring currents, disturbance storm time (*Dst*) perturbation, and solar energetic particle events, while CIR-driven storms have longer duration and hotter plasma sheets.

On the other hand, many studies have examined the role of solar wind parameters in the development of geomagnetic storms. Choi et al. (2008) investigated the statistical characteristics of solar wind dynamic pressure enhancements during geomagnetic storms. In their study, about 81% of storms studied indicate at least one event of dynamic pressure enhancements. Weigel (2010) quantified the influence of solar wind density using two statistical measures, and concluded that the solar wind density modifies the ability of a given value of the solar wind electric field to create a *Dst* perturbation. Lopez et al. (2004) also showed that high solar number density causes a change in the compression ratio of the bow shock for strong and southward IMF, which is typically associated with geomagnetic storms and an enhanced ring current.

It is well known that magnetic storms are caused by enhanced magnetospheric convection during a prolonged period of southward IMF (Burton et al. 1975). On the other hand, Du et al. (2008) studied a geomagnetic storm that occurred on 21-22 January 2005, and found that magnetic storm is highly anomalous because the storm main phase developed during northward IMFs. They have interpreted this case as energy storage in the magnetotail and delayed release into the magnetosphere.

After classifying MC polarity, Echer et al. (2005) presented a statistical study of MC parameters and geoeffectiveness. Considering that the IMF polarity of developing magnetic storms is important, it would be interesting to examine the influence of polarity change during magnetic storms. To identify the dependence of IMF polarity change, magnetic storms are divided into CME-driven storms, CIR-driven storms, and complicated types. Then, variation of magnetic field polarity (B_y, B_z) is analyzed during the main phase of magnetic storms. Echer et al. (2005) utilized only N-S and S-N polarity of MC, but in this research polarity change for the CME and CIR-driven storms is studied separately using the 12 types specified by IMF (B_y, B_z). The statistical relationship between solar wind parameters is also examined, including IMF B_z component and magnetic storms during the storm period by time-integrating. The time-integrated solar wind parameters are compared with the time-integrated *Dst* index during the storm period. The time lag in terms of hour from B_{zmin} to Dst_{min} during the main phases of CME and CIR-driven storms is also investigated.

2. DATA AND METHOD

Hourly average values of solar wind plasma and magnetic field data were obtained from National Aeronautics and Space Administration (NASA)'s OMNIWeb site (http://nssdc.gsfc.nasa.gov/omniweb) during 1997~2003. Magnetic field components are given in the GSM. To analyze the variation of IMF polarity and solar wind parameters, these data are used during the period of magnetic storms. Storms are classified according to their solar wind driver, including CME and CIRs. According to Borovsky & Denton (2006), CME-driven storms include CME sheaths, MC, and ejecta, while CIR-driven storms contain high-speed streams. Sheath fields present in the region between the interplanetary shock and the interplanetary CME (ICME). MC is characterized based on the following criteria: strong magnetic field, rotation of a large angle direction, low proton temperature, and low plasma beta (Burlaga et al. 1981). MC is classified as ejecta if it is hard to identify the rotation of magnetic field (Oh et al. 2007). CIR corresponds to an interaction region between low and high solar wind speed. It is also characterized by high proton temperature, and low number density.

From some reference criteria, CME and CIR-driven storms were selected through an inspection of the data available OMNIWeb site. Through this process, a total of 156 storms were selected from the period of 1997~2003, that is, 109 (69.9%) CME-driven storms, 29 (18.6%) CIR-driven storms, and 18 (11.5%) complicated types. As mentioned above, complicated types were not included in this analysis.

The *Dst* index data for this analysis are provided by the World Data Center for Geomagnetism, Kyoto (http://wdc.kugi.kyoto-u.ac.jp). Storms are divided into three categories in terms of the minimum value of the *Dst* index, Dst_{min}: severe (Dst_{min} < -200 nT), intense (-200 nT ≤ Dst_{min} < -100 nT), moderate (-100 nT ≤ Dst_{min} < -50 nT). A

Table 1. List of magnetic storms used in this study.

Storm / year	Moderate			Intense			Severe			Total		
	CME	CIR	COMP	CME	CIR	COMP	CME	CIR	COMP	CME	CIR	COMP
1997	8	4	0	5	0	0	0	0	0	13	4	0
1998	9	4	3	6	1	1	1	0	0	16	5	4
1999	7	4	0	3	0	0	1	0	0	11	4	0
2000	14	4	1	4	1	0	3	0	0	21	5	1
2001	12	1	3	6	0	0	4	0	0	22	1	3
2002	5	4	5	6	2	0	0	0	0	11	6	5
2003	11	3	5	2	1	0	2	0	0	15	4	5
Total	66	24	17	32	5	1	11	0	0	109	29	18

CME: coronal mass ejection, CIR: co-rotating interaction region, COMP: complicated storm type.

total of 156 magnetic storms, including 11 severe storms, 38 intense storms, and 107 moderate storms, were selected from the period of 1997~2003. Table 1 shows the list of storms used in this study during the main phase of magnetic storms. Assuming that the ring current provides the main contribution to the *Dst* index, *Dst* index is utilized for this analysis. The main phase of a magnetic storm is defined by the interval when the *Dst* index becomes less than -15 nT and reaches to the minimum value, while the late period is from the minimum to the moment when it recovers to -15 nT. As noted above, only magnetic storms with the *Dst* index exceeding -50 nT at the minimum value were used. Furthermore, only clearly recognizable storms with a single minimum and monotonically recovering storms in terms of the *Dst* index were chosen. Thus, the number of storms differs from the data presented in other papers because the criteria for storm selection are different (Choi et al. 2008).

3. RESULTS

3.1 Variation of Magnetic Field (B_y, B_z) Polarity during the Main Phase of Magnetic Storms

Tsurutani et al. (1988) noted that magnetic storms are caused by long duration, intense southward IMFs. As mentioned in the introduction, Du et al. (2008) studied about a storm main phase during northward IMFs. Considering that the direction of IMF is important for magnetic storms, it would be worth investigating the interplanetary conditions of IMF B_y and B_z signs on the development of a storm. For this purpose, the direction change of IMF B_y and B_z components during the main phase of magnetic storm is examined.

Fig. 1 shows temporal variations of (a) B_y, (b) B_z component of IMF, (c) solar wind temperature, (d) solar wind density, (e) solar wind speed, (f) beta, and (g) *Dst* index during 20-25 November 2003. The horizontal axis denotes universal time and the two vertical dashed lines represent the beginning and the maximum epoch of the storm. The dotted lines in Figs. 1a and b represent the zero values of IMF B_y and B_z, respectively. As shown in Figs. 1a and b, the IMF B_y component changes from a positive value to a negative value, and IMF B_z component remains negative during almost all of the main phase. In Fig. 1c, the solar wind temperature is somewhat high in the early stage of the main phase, but immediately becomes low. Values of solar wind density and speed in Figs. 1d and e are higher during the main phase than during the recovery phase. In contrast, the beta of plasma, symbolized by β, is the ratio of the plasma pressure to the magnetic pressure, which is lower during the main phase than during the recovery phase. Considering these conditions, Fig. 1 is an example of magnetic storms driven from MC. As can be seen from in Fig. 1, the *Dst* index decreased rapidly, and the minimum value of -422 nT at 2100 UT was recorded in November 2003.

It is believed that the B_z component of IMF is more important than B_y on the development of magnetic storms. For this reason, B_z component was inserted in the first column of Table 2. Table 2 shows the classification of interplanetary conditions in terms of IMF B_z and B_y signs. F in Table 2 refers to the fluctuation of magnetic field, and the sign of '+ → -' or '- → +' stands for one polarity change. Magnetic storms are classified into 12 types according to IMF signs. No magnetic storm occurred during the positive IMF B_z period in this study. For this reason, those cases are not included in type classifications. As shown in Table 2, when IMF B_z remains steadily negative during the main phase of magnetic storms, they are classified as T1, T2, T3, and T4. A storm is included as one of these types if the percentage of positive values is below 10%. If the polarity of IMF B_z changes once, it

belongs to T5~T8. Accordingly, if IMF B_z fluctuates, that type is one of T9~T12. For example, if the IMF condition is $B_z < 0$ and $B_y > 0$, it belongs to T1. When IMF B_z is fluctuating and $B_y < 0$ during the main phase, type is T10. As can be seen from Table 2, almost half of CME-driven storms examined in this study, 44.2% (61 storms), occurred when IMF B_z remained steadily negative. Fig. 2 shows the histograms for 12 types during the main phase of CME-driven storms with the three storm categories. Since the number of storms in each category is not the same, the vertical axis is expressed in terms of a percentage value. For the CME-driven storms, it is found that the average number of storms for negative sign of IMF B_z (T1~T4) is high, at 56.4%, 53.0%, and 63.7% in each storm category,

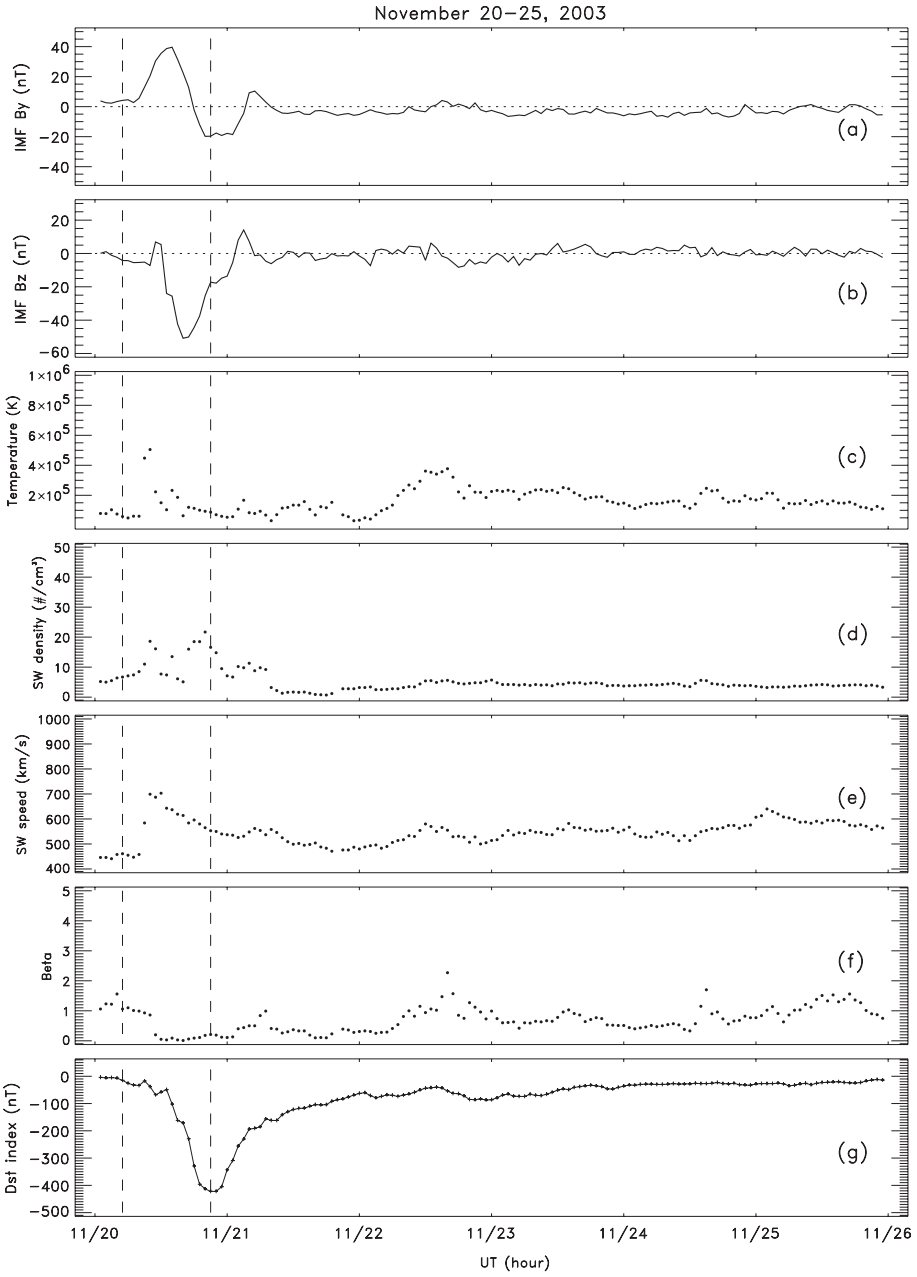

Fig. 1. Temporal variations of (a) B_y, (b) B_z component of IMF, (c) solar wind temperature, (d) solar wind density, (e) solar wind speed, (f) beta, and (g) *Dst* index during 20-25 November 2003. The two vertical dashed lines represent the beginning and the maximum epoch of the storm. The *Dst* index decreased rapidly and recorded the minimum value, -422 nT at 2100 UT on November 2003. IMF: interplanetary magnetic field, *Dst*: disturbance storm time.

Table 2. Classification of interplanetary conditions in terms of IMF B_z and B_y signs.

Magnetic field polarity		Moderate		Intense		Severe		Sum		Total	Type
B_z	B_y	CME	CIR	CME	CIR	CME	CIR	CME	CIR		
+	+	·	·	·	·	·	·	·	·	·	·
+	-	·	·	·	·	·	·	·	·	·	·
+	+ → - - → +	·	·	·	·	·	·	·	·	·	·
+	F	·	·	·	·	·	·	·	·	·	·
-	+	3	1	3	1	1	0	7	2	9	T1
-	-	14	2	3	1	0	0	17	3	20	T2
-	+ → - - → +	13	0	7	0	3	0	23	0	23	T3
-	F	7	4	4	1	3	0	14	5	19	T4
+ → - - → +	+	4	3	2	1	0	0	6	4	10	T5
+ → - - → +	-	3	0	1	0	0	0	4	0	4	T6
+ → - - → +	+ → - - → +	4	1	1	0	0	0	5	1	6	T7
+ → - - → +	F	4	2	2	0	1	0	7	2	9	T8
F	+	4	6	2	0	0	0	6	6	12	T9
F	-	1	2	1	0	0	0	2	2	4	T10
F	+ → - - → +	4	1	4	0	1	0	9	1	10	T11
F	F	5	2	2	1	2	0	9	3	12	T12
Total		66	24	32	5	11	0	109	29	138	

IMF: interplanetary magnetic field, CME: coronal mass ejection, CIR: co-rotating interaction region.

respectively. For the moderate storms, T2 shows the highest number of storms, while T3 has the highest percentage value for intense and severe storms. In particular, the sum of T3 and T4 for the severe storms is more than half in CME type storms. It is noted that IMF B_z seems to play a more important role in developing magnetic storms than B_y on the basis of Table 2 and Fig. 2. However, fluctuation of B_y component also seems to be important for big storms.

On the other hand, the results for CIR-driven storms are different from those for the CME storm type. As shown in Fig. 3, the percentage of storms for T1~T4 is found to be low, at 29.2%, compared to that of T9~T12, which is 45.8% for moderate storms. When the condition is $B_z < 0$, the number of storms for CIR-driven type is approximately 52% lower than that of CME type for moderate storms. It was impossible to analyze storms this severe because there was no this category in CIR-driven type. For CIR-driven storms, a wide range of numbers was recorded for moderate storms, while there is no distribution in several types for intense storms.

3.2 Correlations between the Time-Integrated *Dst* Index and Solar Wind Parameters during the Main Phase

Echer et al. (2008) investigated the dependence of peak *Dst* on interplanetary parameters. This study also investigated the relationship between the magnetic storms and solar wind parameters. Taking into account the fact that the values of several solar wind parameters are temporary phenomena while a magnetic storm is continuous, it may be reasonable to compare time-integrated parameters rather than individual parameters. Thus, the difference between the present study and others is that the correlation used the time-integrated values is examined. In addition, I analyzed magnetic storms after dividing them into CME-driven storm and CIR-driven storms.

Fig. 4 shows the correlations between the time-integrated *Dst* index and various solar wind parameters for the CME-driven storms: (a) time-integrated IMF B_z, (b) time-integrated temperature, (c) time-integrated solar wind density, and (d) time-integrated solar wind speed. 'r ' in each figure stands for correlation coefficient, and each filled circle represents one magnetic storm. As shown in Fig. 4a, the correlation coefficient is highest, at 0.77, between the time-integrated IMF B_z component and time-integrated *Dst* index during the main phase of magnetic storms. These indicate that IMF B_z is closely associated with the development of magnetic storms during

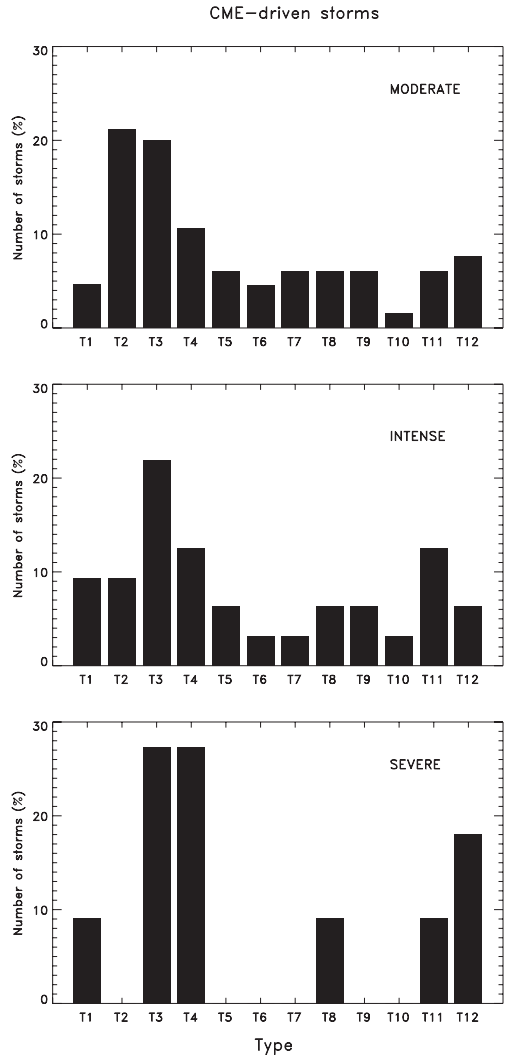

Fig. 2. Histograms for 12 types for CME-driven storms with the three storm categories. Since the number of storms for each category is not the same, the vertical axis is expressed in terms of percentage values. CME: coronal mass ejection.

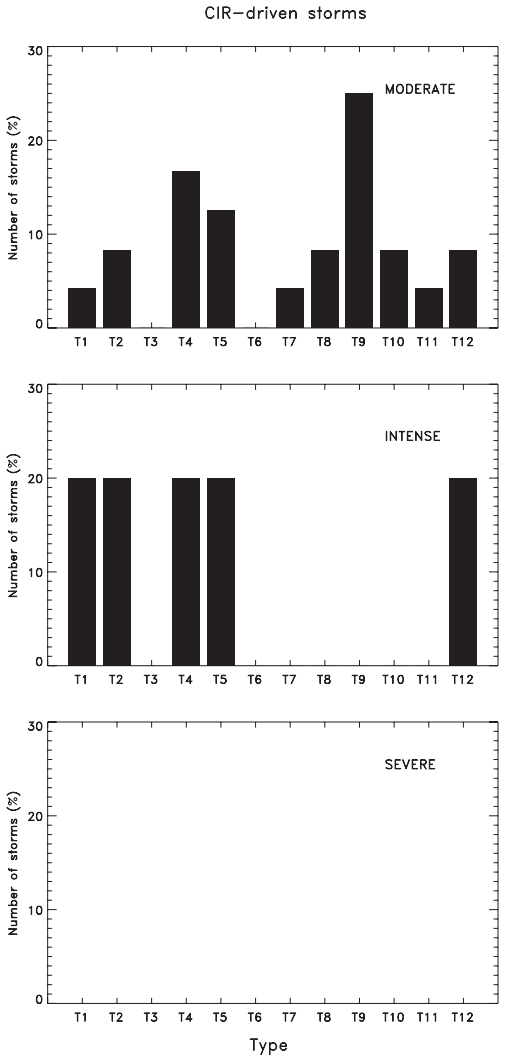

Fig. 3. Same as Fig. 2 but for CIR-driven storms. CIR: co-rotating interaction region.

the main phase for the CME-driven storms. On the other hand, no direct relation seems to exist between time-integrated temperature and time-integrated *Dst* index during the main phase. Fig. 5 shows the correlations for the CIR-driven storms. The vertical and horizontal axes of (a)~(d) indicate the same as Fig. 4. The highest correlation is found, with the correlation coefficient being 0.93, between time-integrated *Dst* index and time-integrated solar wind speed. In Fig. 5a, the correlation coefficient is lower than the coefficient of CME type.

Table 3 shows the average values between the properties of CME-driven storms and CIR-driven storms. As can be seen from Table 3, for the CME-driven storms, $|Dst_{min}|$ for the CME-driven storms is 34% higher than that of the CIR-driven storms, and $|B_{zmin}|$ is also higher than for the CIR-driven type. Duration and time lag for the main phase is longer for the CIR-driven storms than for the

Table 3. The average values between the properties of CME-driven storms and CIR-driven storms.

Average values	CME-driven storms	CIR–driven storms
Dst_{min} (nT)	-103.6	-77.5
Duration (hour)	9.7	11.3
B_{zmin} (nT)	-12.9	-10.3
Proton temperature (K)	177,204	214,337
SW density (#/cm^3)	10.0	10.1
Beta (β)	0.79	1.03
Time lag (hour)	3.86	5.46

CME: coronal mass ejection, CIR: co-rotating interaction region.

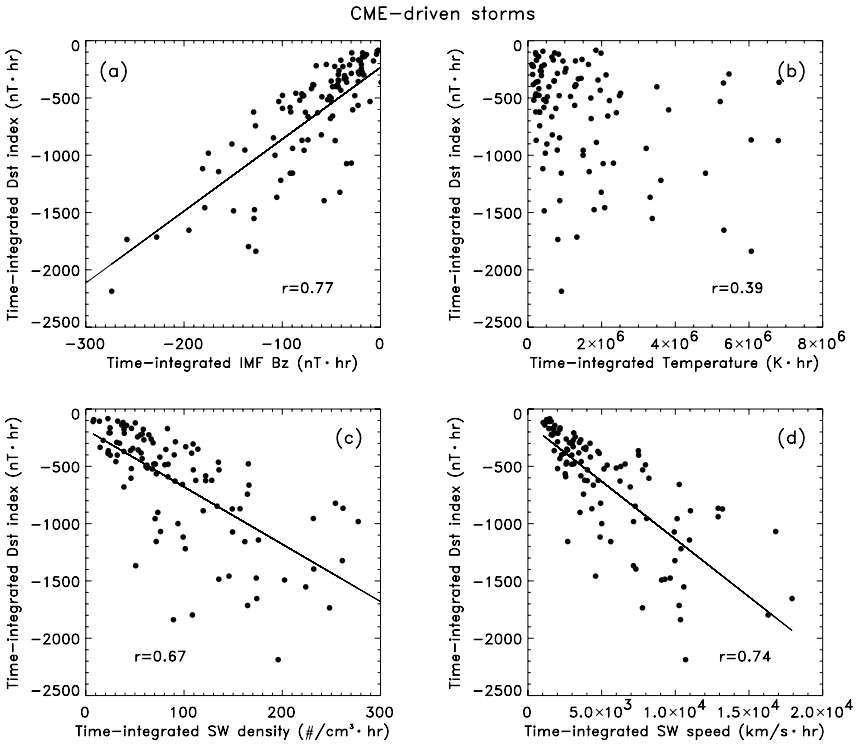

Fig. 4. The correlations between the time-integrated *Dst* index and various solar wind parameters for the CME-driven storms: (a) time-integrated IMF B_z, (b) time-integrated temperature, (c) time-integrated solar wind density, and (d) time-integrated solar wind speed. 'r ' in each figure stands for correlation coefficient. Each filled circle represents one magnetic storm. *Dst*: disturbance storm time, CME: coronal mass ejection, IMF: interplanetary magnetic field.

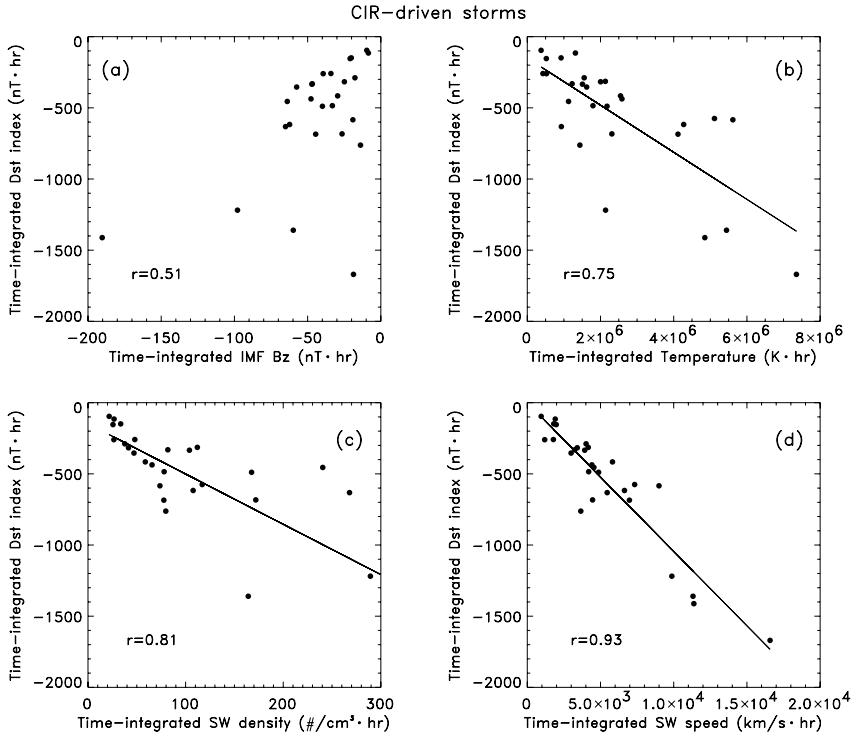

Fig. 5. Same as Fig. 4 but for CIR-driven storms. CIR: co-rotating interaction region.

CME-driven storms. Also, temperature for the CIR-driven storms is higher than that of the CME-driven storms. Average beta (β) is low, at 0.79, for CME-driven storms while beta is above 1.00 for the CIR-driven storms. These results correspond to the results obtained by Borovsky & Denton (2006). According to Borovsky & Denton (2006), plasma density is described as more superdense for CME-driven storms than for CME-driven storms. However, plasma density for the CME storms is similar to the CIR-driven type in the present work. This may be due to the selection criteria and periods used.

3.3 Time Lag with Storm Size for CME-Driven Storms and CIR-Driven Storms

Fig. 6 shows the relationship between Dst_{min} and B_{zmin} during the main phase for the CME-driven storms and CIR-driven storms. It would be meaningful to point out that the slopes of the linear regression lines for the two cases are different. The relationships between Dst_{min} and B_{zmin} during the main phase are expressed as follows:

$$Dst_{min} = 7.3\ (B_{zmin}) - 9.36 \quad (1)$$

$$Dst_{min} = 3.9\ (B_{zmin}) - 37.2 \quad (2)$$

Eqs. (1) and (2) are for the CME-driven storms and CIR-driven storms. Compared with Figs. 6a and b, the slope in Fig. 6a is about two times higher than that of Fig. 6b. When B_{zmin} value is -20 nT, the corresponding Dst_{min} values are -155.4 nT and -115.2 nT for the CME and CIR storms, respectively. This means that IMF B_z for the CME-driven storms is more efficient than for the CIR-driven storms on the development of magnetic storms. The correlation coefficient for the CME-driven storms is significantly high, at 0.90, compared to for the CIR-driven storms.

Fig. 7 shows the comparison of time lag for the CME

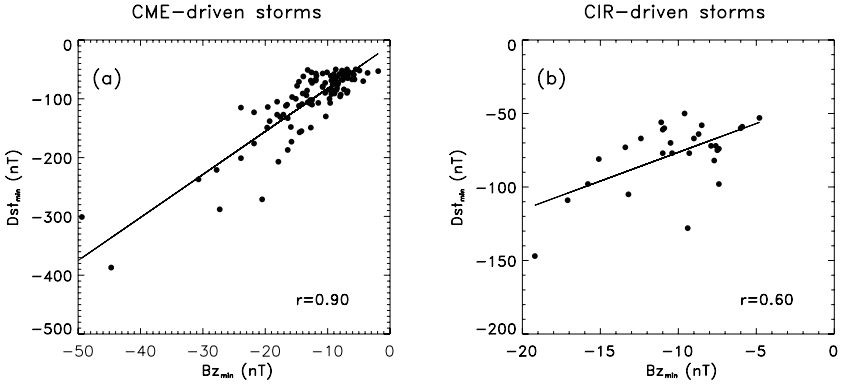

Fig. 6. The relationship between Dst_{min} and B_{zmin} during the main phase for the CME and CIR-driven storms. CME: coronal mass ejection, CIR: co-rotating interaction region.

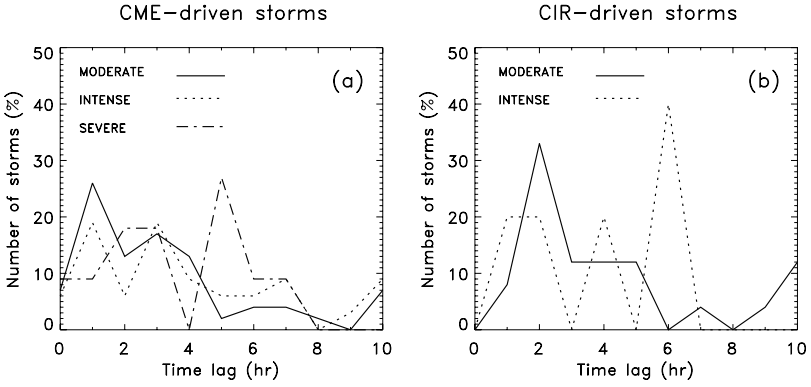

Fig. 7. Comparison of time lag with storm size for the CME and CIR-driven storms. CME: coronal mass ejection, CIR: co-rotating interaction region.

and CIR-driven storms with storm size. For the CME-driven storms, time lag of 26% moderate storms is one hour, whereas time lag of 33% moderate storms is two hour for the CIR-driven storms. The pattern of intense storms is similar to that of moderate storms for the CME-driven storms, but the pattern of time lag for the severe storms is different. For CIR-driven storms, time lag of moderate storms is concentrated on two hours whereas that of intense storms is longer.

4. SUMMARY AND DISCUSSION

In this research, the manner in which the direction change of IMF B_y and B_z components (in GSM coordinate) during the main phase is related with the development of storms was examined. These were classified into 12 types according to the direction change of IMF B_y, B_z during the storm periods. Time-integrated solar wind parameters are compared to the time-integrated *Dst* index during the main phase for CME and CIR-driven storms, respectively. The differences between CME-driven storms and CIR-driven storms were also discussed.

Several interesting results were summarized, and their implications briefly discussed. For the CME-driven storms, under steady conditions of $B_z < 0$, the number of storms represents more than half of storms. The percentage of storms was 56.4%, 53.0%, and 63.7% by storm category, respectively. One can note that the direction of B_z plays a more important role in the development of magnetic storms than B_y. However, for the CIR-driven storms, the number of moderate storms was only 29.2%, while the number of intense storms was over half (60.0%) under the $B_z<0$ condition. For CIR-driven storms, a wide range of numbers was recorded for the moderate storms, but there is no distribution in several types for the intense storms. Also, the fluctuations of IMF B_y and B_z components seem to be associated with the development of magnetic storms.

The correlation coefficient is highest, at 0.77, between the time-integrated IMF B_z component and time-integrated *Dst* index for CME-driven storms, whereas the highest correlation is found, with a correlation coefficient of 0.93, between time-integrated *Dst* index and time-integrated solar wind speed for CIR-driven storms.

The correlation coefficient between Dst_{min} and B_{zmin} is higher for the CME-driven storms than for the CIR-driven storms. Considering their slopes, IMF B_z of the CME-driven storms is more efficient on developing magnetic storms. Average time lag for the CIR-driven storms is longer than for CME-driven storms, and showed different aspects as shown in Fig. 7. As mentioned previously, Borovsky & Denton (2006) compared the properties between CME-driven storms and CIR-driven storms. In the present study, the results are approximately in accordance with Borovsky & Denton (2006), except for the solar wind density. This may be due to the period of data used and the criteria for storm selection.

ACKNOWLEDGMENTS

I would like to thank the World Data Center for Geomagnetism-Kyoto for *Dst* index information, and the National Space Science Data Center for OMNI solar wind data.

REFERENCES

Borovsky JE, Denton MH, Differences between CME-driven storms and CIR-driven storms, JGR, 111, 11447-11463 (2006). doi: 10.1029/2005JA011447

Burlaga L, Sittler E, Mariani F, Schwenn R, Magnetic loop behind an interplanetary shock: Voyager, Helios, and IMP 8 observations, JGR, 86, 6673-6684 (1981). doi: 10.1029/JA086iA11p08893

Burton RK, McPherron RL, Russell CT, An empirical relationship between interplanetary conditions and *Dst*, JGR, 80, 4204-4214 (1975). doi: 10.1029/JA080i031p04204

Choi C-R, Kim K-C, Lee D-Y, Kim J-H, Lee E, Statistical characteristics of solar wind dynamic pressure enhancements during geomagnetic storms, JASS, 25, 113-128 (2008). doi: 10.5140/JASS.2008.25.2.113

Du AM, Tsurutani BT, Sun W, Anomalous geomagnetic storm of 21-22 January 2005: a storm main phase during northward IMFs, JGR, 113, 13284-13292 (2008). doi: 10.1029/2008JA013284

Echer E, Alves MV, Gonzalez WD, A statistical study of magnetic cloud parameters and geoeffectiveness, JASTP, 67, 839-852 (2005). doi: 10.1016/j.jastp.2005.02.010

Echer E, Gonzalez WD, Tsurutani BT, Gonzalez ALC, Interplanetary conditions causing geomagnetic storms (*Dst* ≤ -100 nT) during solar cycle 23 (1996-2006), JGR, 113, 12744-12759 (2008). doi: 10.1029/2007JA012744

Lopez RE, Wiltberger M, Hernandez S, Lyon JG, Solar wind density control of energy transfer to the magnetosphere, GeoRL, 31, 8804-8807 (2004). doi: 10.1029/2003GL018780

Oh SY, Yi Y, Kim YH, Solar cycle variation of the interplanetary forward shock drivers observed at 1 AU, SoPh, 245,

391-410 (2007). doi: 10.1007/s11207-007-9042-2

Tsurutani BT, Gonzalez WD, Tang F, Akasofu SI, Smith EJ, Origin of interplanetary southward magnetic fields responsible for major magnetic storms near solar maximum (1978-1979), JGR, 93, 8519-8531 (1988). doi: 10.1029/JA093iA08p08519

Weigel RS, Solar wind density influence on geomagnetic storm intensity, JGR, 115, 15062-15072 (2010). doi: 10.1029/2009JA015062

Wu C-C, Lepping RP, Solar cycle effect on geomagnetic storms caused by interplanetary magnetic clouds, AnGeo, 24, 3383-3389 (2006). doi: 10.5194/angeo-24-3383-2006